Supporting information

Iron Oxide Encapsulated Titanium Niobate Nanotubes as High-Performance Lithium-Free Anode for Solid-State Batteries

Wei Wu,[#1,2] Wang Lin, [#1] Hongjiang Chen, [1] Keyan Wei, [1] Zhitong Li, [1] Haitao Yang, [1] Mingxian Liu, [1] Huaicheng Xiang[1], Libo Deng[2] and Lei Yao[*1]*

[1] Shenzhen Key Laboratory of Special Functional Materials, Shenzhen Engineering Laboratory for Advanced Technology of Ceramics, Guangdong Research Center for Interfacial Engineering of Functional Materials, College of Materials Science and Engineering, Shenzhen University, Shenzhen 518060, P. R. China

[2] College of Chemistry and Environmental Engineering, Shenzhen University, Shenzhen 518060, China

[#] These authors (W. Wu and W. Lin) contributed equally to this work.

[*] Corresponding author:

E-mail address: lyao@szu.edu.cn (L. Yao)

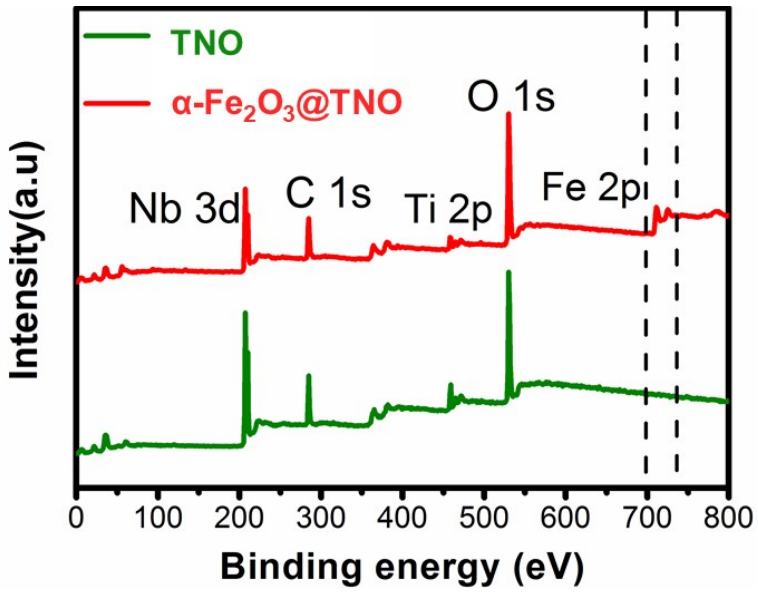

Figure S1. Wide-scan XPS survey of α-Fe_2O_3@TNO nanofibers and TNO nanofibers.

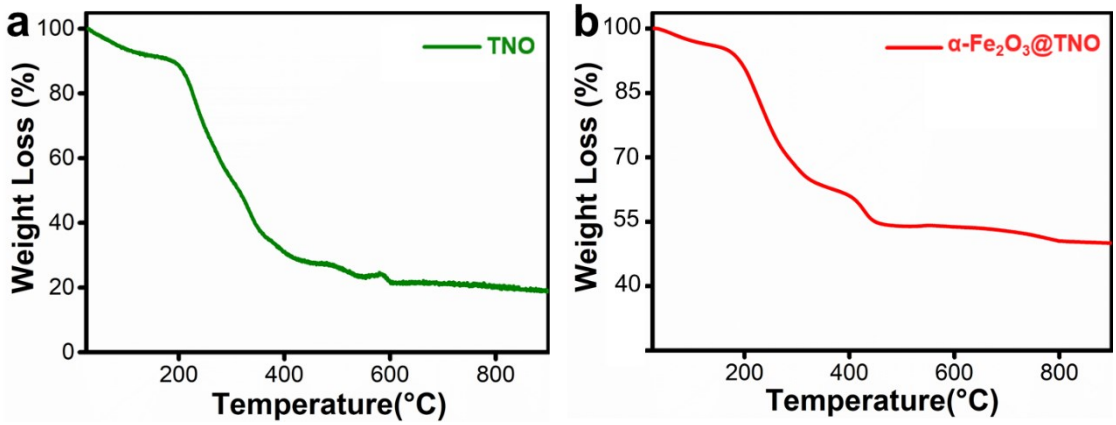

Figure S2. TGA curves of (a) TNO and (b) α-Fe_2O_3@TNO nanofibers.

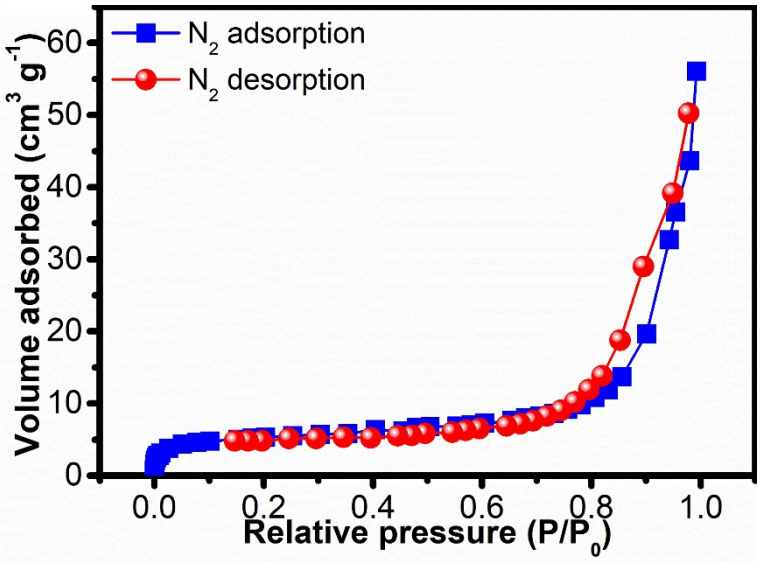

Figure S3. Nitrogen sorption isotherm of the α-Fe_2O_3@TNO nanofibers.

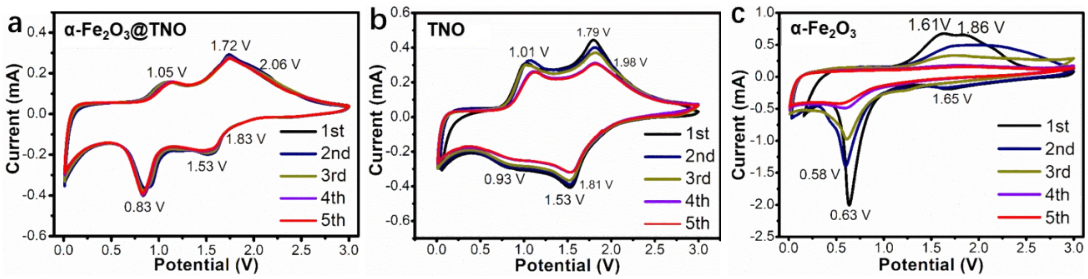

Figure S4. CV curves of (a) α-Fe_2O_3@TNO, (b) TNO, and (c) α-Fe_2O_3 electrodes at a scan rate of 0.1 mV s^{-1} measured in the voltage range of 0.01-3.0 V for the initial 5 cycles.

In the cathodic and anodic sweeps of α-Fe_2O_3@TNO (Fig. S2a), the peak couples at 1.53/1.72 V, 1.83/2.06 V, and 0.83/1.05 V can be attributed to the valence variations of Nb^{5+}/Nb^{4+}, Ti^{4+}/Ti^{3+}, and Nb^{4+}/Nb^{3+} redox couples due to the insertion and extraction of Li^+ in TNO (Fig. S2b).[1] Moreover, the sharp peak at 0.83 V also corresponds to the Fe^0/Fe^{3+} (Fe^{2+}) redox couples, originating from the phase transition from α-Fe_2O_3 to $Li_xFe_2O_3$, subsequently to cubic $Li_2Fe_2O_3$, and finally to the complete reduction to Fe^0 and then in reverse.[2] The plateau voltage for the α-Fe_2O_3@TNO nanofibers is higher than that for the α-Fe_2O_3 nanoparticles in Fig. S2c, where a clear decrease from 0.63 to 0.58 V is observed after only 5 cycles, indicating the greatly improved conductivity and kinetics of α-Fe_2O_3 in the composite nanofibers.[3] Moreover, the intensity and peak positions for the α-Fe_2O_3@TNO nanofibers only showed slight changes within the initial 5 cycles, signifying the good stability and reversibility of the electrochemical reactions in the composite.

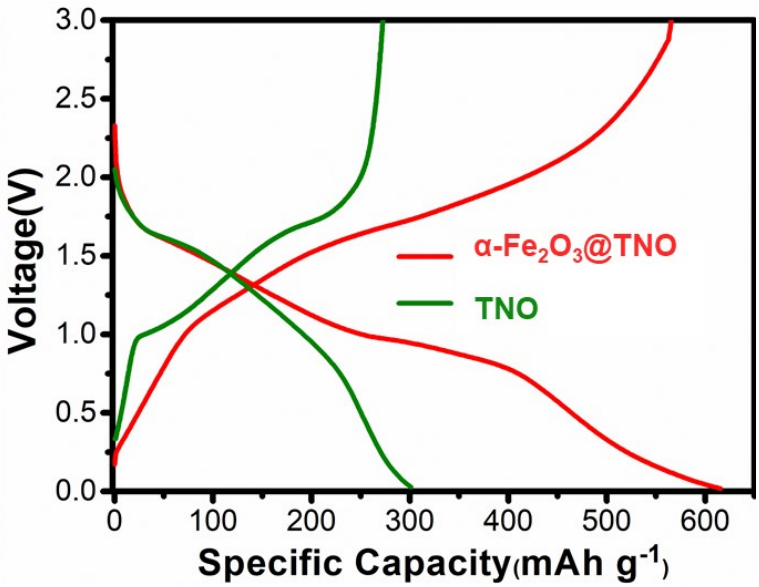

Figure S5. Discharge/charge curves of α-Fe_2O_3@TNO and TNO for the first cycle at 0.1 A g^{-1} from 0.01-3.0 V.

The discharge curve of α-Fe_2O_3@TNO can be divided into four plateau regions: (1) between 2.0 and 1.7 V, (2) at ≈1.6 V, (3) between 1.2 and 0.7 V, and (4) a further sloping region down to 0.01 V, representing different stages upon Li^+ insertion. Typically, the plateau between 1.2 and 0.7 V corresponds to the lithiation of α-Fe_2O_3. In contrast, the TNO electrode displays only three discharge plateau regions with a generally constant decline below ≈1.5 V in the absence of α-Fe_2O_3. These results are consistent with the CV analysis in Fig. S2.

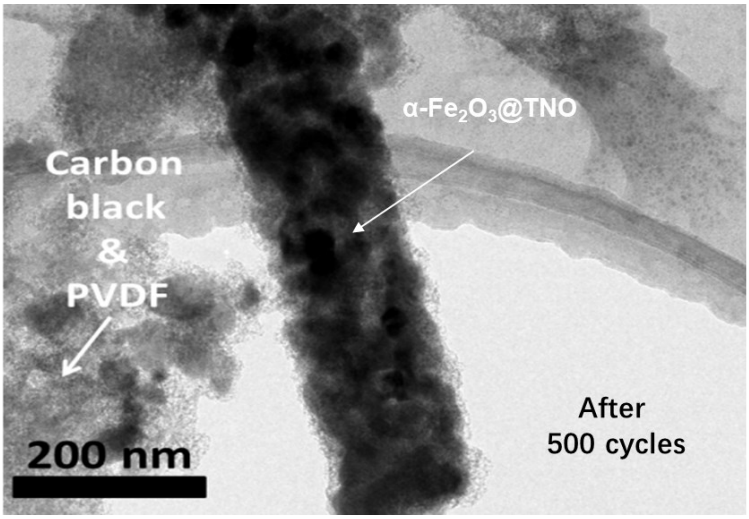

Figure S6. TEM image of α-Fe_2O_3@TNO nanofiber after 500 cycles.

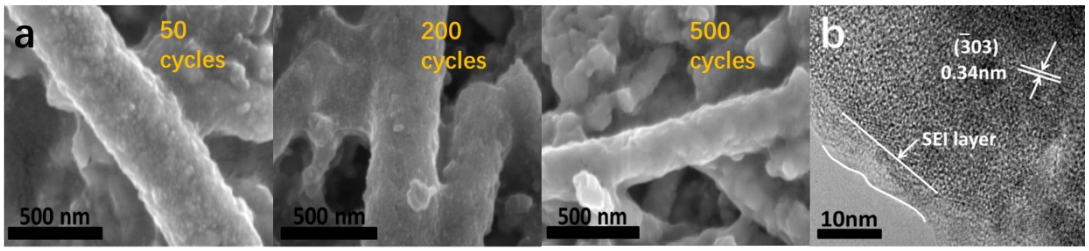

Figure S7. SEM images of (a) α-Fe_2O_3@TNO electrode after 50, 200, and 500 cycles and (b) HRTEM image of α-Fe_2O_3@TNO nanofiber after 500 cycles.

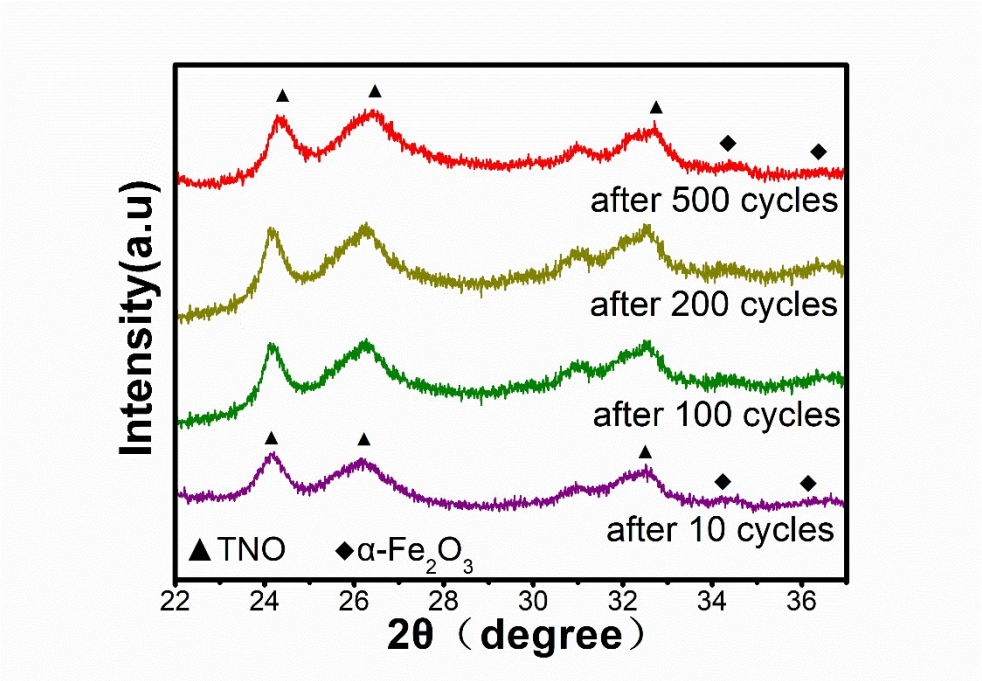

Figure S8. XRD patterns of α-Fe_2O_3@TNO electrode after 20, 100, 200, and 500 cycles.

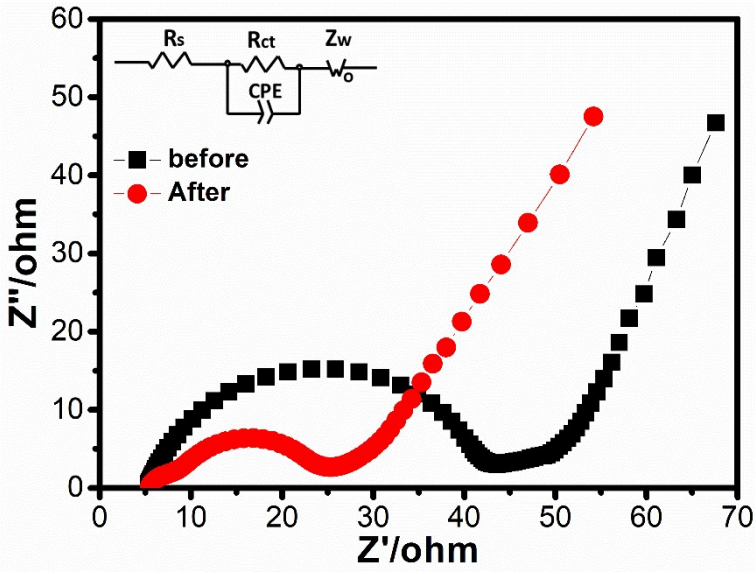

Figure S9. Fitted Nyquist plots of α-Fe_2O_3@TNO electrode before and after rate capability test.

Each plot consists of semicircles in the high-medium-frequency region (Rs and the Rct/CPE pair) and one slope in the low-frequency region (Zw), representing the interfacial resistance/charge-transfer resistance and Li^+ diffusion in the bulk particle, respectively.[4] The fitted resistance values for α-Fe_2O_3@TNO electrode before and after the rate capability test were 25.8 and 44.5 Ω. This indicates a faster electrochemical kinetics after the activation of the α-Fe_2O_3@TNO electrode through the rate capability test.[5]

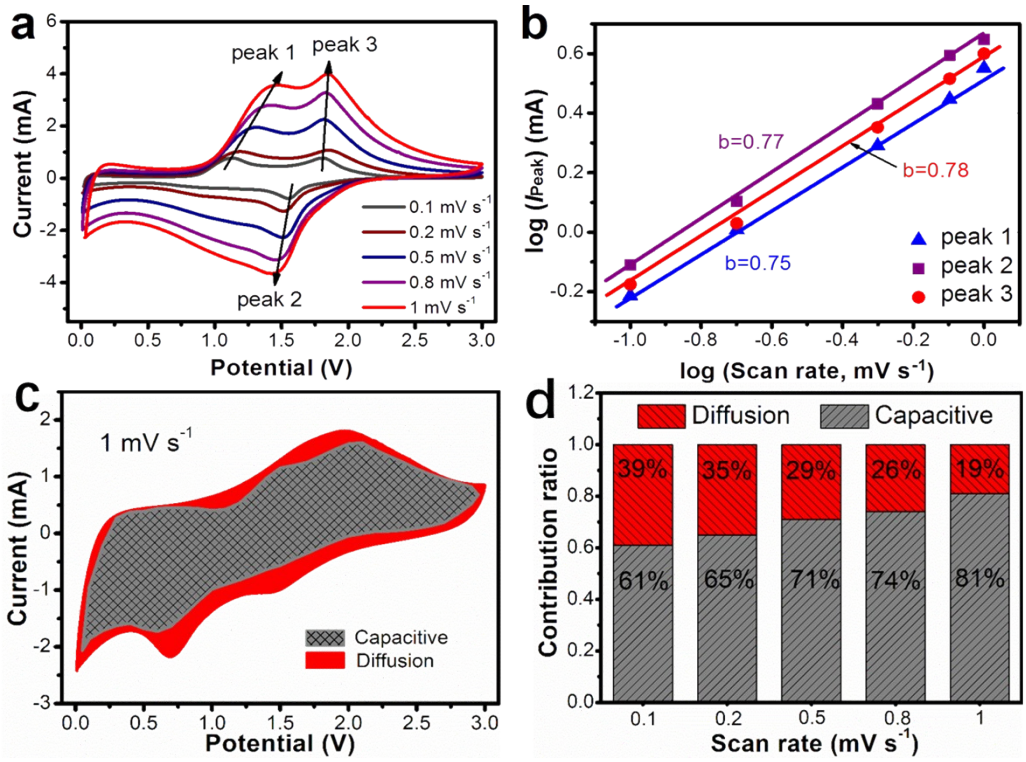

Figure S10. (a) CV curves of TNO electrode at scan rates from 0.1 to 1.0 mV s^{-1} and (b) logarithmic relationship between the peak current and scan rate, (c) CV curves with the separation between total current (red region) and capacitive current (shaded region) at a scan rate of 1.0 mV s^{-1}, and (d) normalized contribution ratio of capacitive capacity at different scan rates.

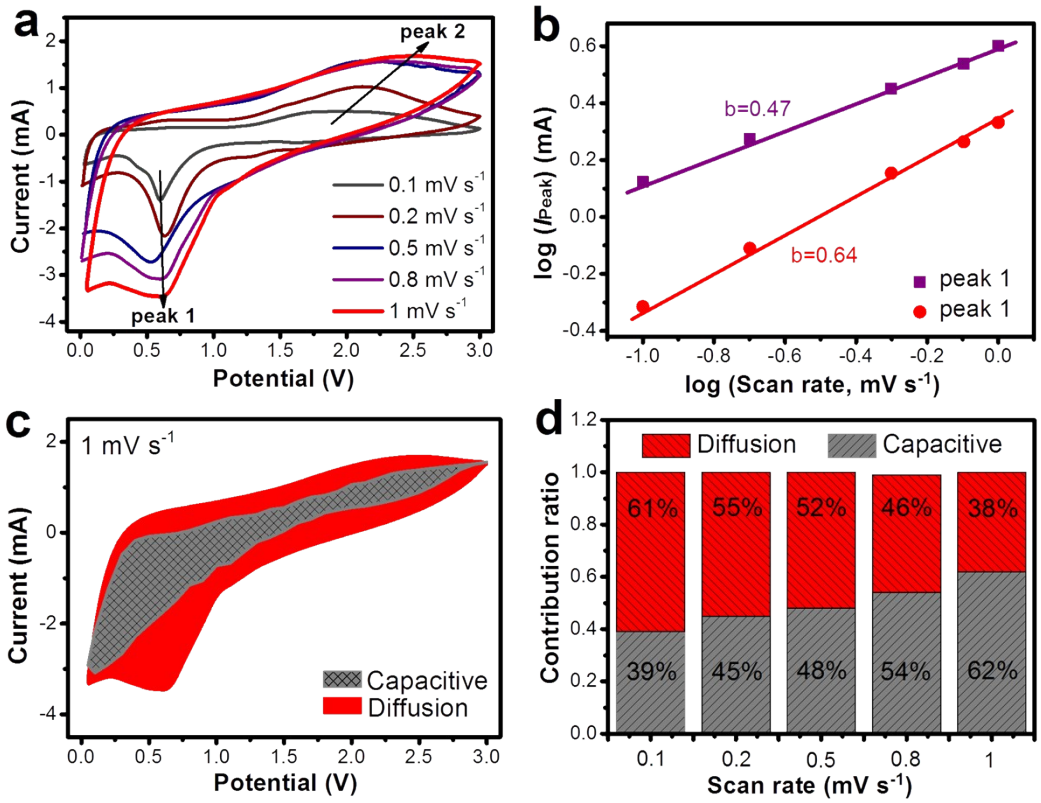

Figure S11. (a) CV curves of α-Fe_2O_3 electrode at scan rates from 0.1 to 1.0 mV s^{-1} and (b) logarithmic relationship between the peak current and scan rate, (c) CV curves with the separation between total current (red region) and capacitive current (shaded region) at a scan rate of 1.0 mV s^{-1}, and (d) normalized contribution ratio of capacitive capacity at different scan rates.

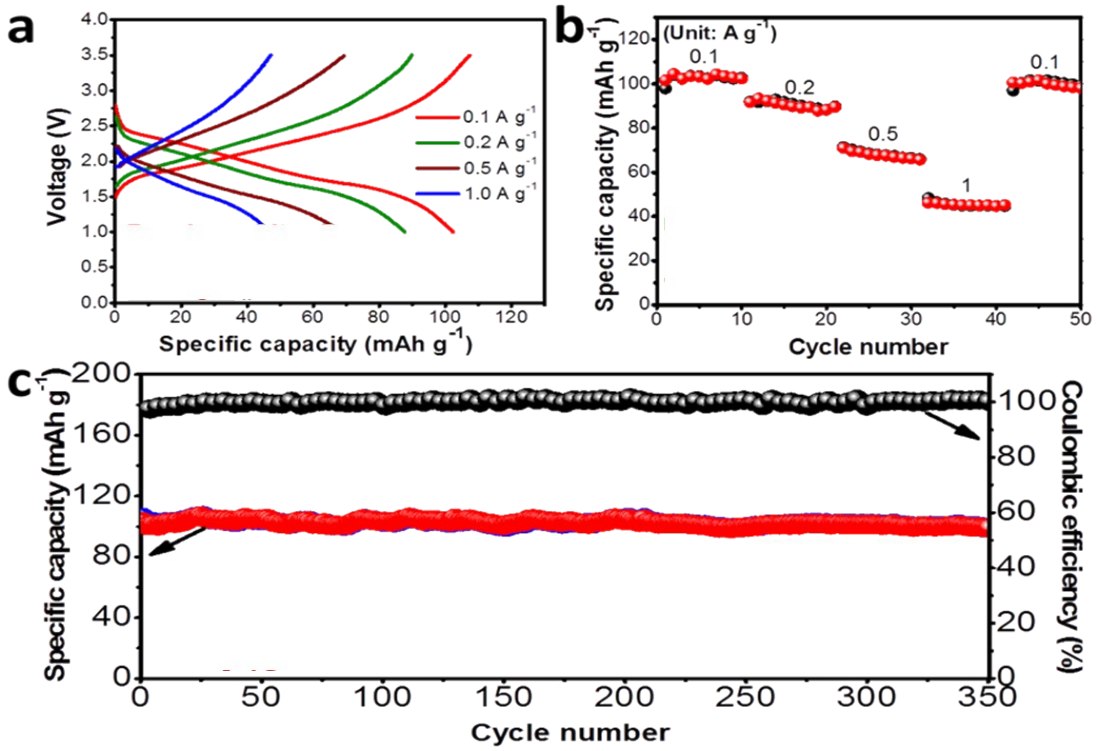

Figure S12. (a) Discharge/charge curves and (b) rate performance of Fe_2O_3@TNO/SSE/LFP SSB pouch full cell at current densities between 0.1 and 1.0 A g^{-1} and (c) its long-term cycling performance at 0.1 A g^{-1}.

Table S1. Electrochemical properties of representative TNO-based anodes reported recently in comparison with this work.

Materials	Specific current (mA g^{-1})	Cycle number	Retained specific capacity (mAh g^{-1})	Capacity retention	Fading rate (per cycle)	Ref.
Porous TNO	388	1000	~190	84.0%	0.016%	[6]
Porous TNO nanotubes	388	700	~220	88.0%	0.017%	[7]
TNO/Graphene fibers	500	100	195	~76.0%	0.240%	[1]
TNO/Graphene	388	300	200	72.7%	0.091%	[8]
Hollow TNO@C spheres	97	500	225	75.0%	0.050%	[9]
TNO hollow nanofiber	155	150	210	70.0%	0.200%	[10]
Nb_2O_5/TNO spheres	388	100	247	89.8%	0.102%	[11]
Mo-doped TNO	194	10	~300	N/A	N/A	[12]
Hierarchical MoS_2/TNO hetero-nanostructure	1000	200	740	91.6%	0.042%	[13]
α-Fe_2O_3@TNO	500	500	423	79.2%	0.042%	This work
	100	80	611	97.6%	0.028%	

References

1. X. Wang and G. Shen, *Nano Energy*, 2015, **15**, 104-115.
2. C. Li, A. Sarapulova, Z. Zhao, Q. Fu, Vanessa Trouillet, A. Missiul, E. Welter and S. Dsoke, *Chem. Mater*, 2019, **31**, 5633-5645.
3. K. Cao, L. Jiao, H. Liu, Y. Liu, Y. Wang, Z. Guo and H. Yuan, *Adv. Energy Mater.*, 2015, **5**, 1401421.
4. Q. Fu, R. Li, X. Zhu, G. Liang, L. Luo, Y. Chen, C. Lin and X. S. Zhao, *J. Mater. Chem. A*, 2019, **7**, 19862-19871.
5. Q. Fu, X. Zhu, R. Li, G. Liang, L. Luo, Y. Chen, Y. Ding, C. Lin, K. Wang and X. S. Zhao, *Energy Storage Mater.*, 2020, **30**, 401-411.
6. H. Park, D. H. Shin, T. Song, W. I. Park and U. Paik, *J. Mater. Chem. A*, 2017, **5**, 6958-6965.
7. A. G. Ashish, P. Arunkumar, B. Babu, P. Manikandan, S. Sarang and M. M. Shaijumon, *Electrochim. Acta*, 2015, **176**, 285-292.
8. G. Zhu, Q. Li and R. Che, *Chem.* 2018, **24**, 12932-12937.
9. H. Yu, H. Lan, L. Yan, S. Qian, X. Cheng, H. Zhu, N. Long, M. Shui and J. Shu, *Nano Energy*, 2017, **38**, 109-117.
10. S. Yoon, S. Y. Lee, T. L. Nguyen, I. T. Kim, S.-G. Woo and K. Y. Cho, *J. Alloys Compd.*, 2018, **731**, 437-443.
11. H. Song and Y. T. Kim, *Chem. Commun.*, 2015, **51**, 9849-9852.
12. C. Pham, J. H. Choi, J. Yun, A. S. Bandarenka, J. Kim, P. V. Braun, S. Y. Jeong and C. R. Cho, *ACS Nano*, 2017, **11**, 1026-1033.